Supporting Information

Tworowski et al. 10.1073/pnas.1414852112

SI Materials and Methods

Data Collection and Structure Determination. Data were collected at the synchrotron radiation source at European Synchrotron Radiation Facility, ID-14 station, France, and with an in-house Rigaku R-axis IV++ image plate detector. Before flash cooling, soaked crystals were transferred into a cryoprotectant containing 30% (vol/vol) glycerol. Diffracted intensities were evaluated and integrated using an HKL2000 package (1), and further scaled using programs from the CCP4 package. Data collection statistics are summarized in Table S1.

The crystal structure of *Tt*PheRS (2) (accession code 1PYS in the Protein Data Bank) was used as a starting model. After rigid body refinement, and cycles of simulated annealing and conjugate gradient minimization, a difference Fourier map with coefficients ($F_{obs} - F_{calc}$) was calculated. The refinement and map calculation were carried out with a CNS package (3). A random sample set containing 5% of the reflections was excluded from the refinement and used for R_{free} calculation. All calculations were performed against the F_{obs} data sets for a *Tt*PheRS–puromycin complex at 50–2.6 Å resolution.

The ligand was built into the electron density, manually adjusted with the program O (4), and regularized using QM/MM (MOPAC2012) (5). Refinement statistics are represented in Table S1. Molecular graphics pictures were prepared with the PyMOL (6) and Chimera programs (7).

Isothermal Titration Calorimetry. The in vitro binding of puromycin to *Ec*PheRS was detected by isothermal titration calorimetry (ITC), using an ITC200 titration microcalorimeter (Microcal; GE Healthcare).

The sample cell (204 μL) was maintained at 25 °C and filled with an 8-μM *Ec*PheRS (heterodimer) solution containing 50 mM Tris·HCl, pH 8.0, 0.2 M NaCl, 5 mM β-mercaptoethanol. The injection syringe was filled with 2.5 mM puromycin solution. During the titration experiments, the sample solution was stirred at 1,000 rpm with the injection syringe. After establishment of a stable baseline, 0.4 μL of solution was injected, to remove possible air bubbles at the syringe opening. Subsequently, a series of 20 microinjections of 1.8 μL of the puromycin solution was made, with each injection separated by 3 min, to enable the heat signal to return to baseline levels. Isothermal titration curves were recorded and analyzed with ORIGIN software (Microcal, Inc.) provided with an ITC instrument.

Microscale Thermophoresis. Microscale thermophoresis (MST) measurements were carried out on a Monolith NT.115 MST instrument (NanoTemper Technologies, GmbH). *Ec*PheRS was labeled with the NT647 fluorescent dye and applied at a final concentration of 100 μM in a solution containing 50 mM Tris·HCl, pH 8.0, 0.2 M NaCl, 10 mM $MgCl_2$, 0.05% Tween 20. Puromycin solution at a concentration of 35 mM (prepared in the same buffer as the protein) was mixed with the protein solution to yield 12 samples containing constant concentration of the labeled protein (50 μM) and varying concentrations of puromycin (17.5 mM to 4.2 μM). Measurements were carried out in hydrophilic capillaries. A dissociation constant of 0.22 mM was determined.

QM/MM Simulations. To generate the conformation of the corresponding ester analog and its structural variants, we applied a combined QM/MM approach, enabling the modeling of enzymatic reactions at a reasonable computational effort, while providing the necessary accuracy (8, 9).

Upon completion of construction (and before QM/MM computations), substrate models were minimized in 500 steps, using an MM3 force field and the steepest descent algorithm, followed by 250 cycles of conjugate gradient minimization (10). Harmonic restraints [50 kcal/(mol·Å)] were used to "lock" the positions of the protein atoms. TINKER 4.3 molecular modeling software (dasher.wustl.edu/tinker/) was used in the MM minimization protocol. Semiempirical QM calculations were performed using a MOPAC2012 package (11).

Structure of the Cyclic 2′,3′-Orthoester. The structure of the cyclic 2′,3′-orthoester was constructed, using the atomic coordinates of the tyrosyl-3′-ribose ester. Hybridization states of carbon (sp^2) and oxygen (sp^2) in the carbonyl group were changed to sp^3. The hydrogen atom at the ribose O2′ was removed. The ortho-OH group was constructed by adding the hydrogen atom to the carbonyl oxygen. The force-field parameters of the single covalent bond were applied to the ribose O2′ and the carbonyl carbon atom pair.

QM/MM Protocol. The reactive region of the *Tt*PheRS subjected to QM computations involves puromycin/ester, the amino acid residues Hisβ261, Asnβ250, Thrβ249, Ileβ242, Valβ246, Aspβ247, Proβ259, Metβ260, Alaβ262, Pheβ263, Leuβ286, Valβ324, Gluβ334, and Alaβ356, and the water molecules W40, W23, and W13.

The charge of the QM system is −1, in the event of Hisβ261 being neutral, and 0 in the protonated state. The MM subsystem was modeled with the MM3pro force field. QM/MM calculations were carried out with the MOPAC2012 code. Interactions between the QM and the MM systems were defined by PM7 Hamiltonian electrostatic coupling scheme (12).

Editing Pathway Calculations. The initial conformations of tyrosyl-3′-ribose ester, cyclic 2′,3′-orthoester, and tyrosyl-2′-ribose ester were optimized in the presence of protein side chains and the water molecules W40, W23, and W13, using the QM/MM protocol as described above. The following reactions were studied: (reaction a) nucleophilic attack of W40 on the carbonyl group of the tyrosyl-3′-ribose ester; (reaction b) isomerization of tyrosyl-3′-ribose ester to cyclic 2′,3′-orthoester; (reaction c) isomerization of cyclic 2′,3′-orthoester to tyrosyl-2′-ribose ester; and reaction d) nucleophilic attack of W40 on the carbonyl group of tyrosyl-2′-ribose ester.

In the isomerization reactions b and c, two optimized reaction end point structures were used in the linear interpolation scheme.

Upon nucleophilic attack of W40 (reactions a and d), the interatomic distance between the electronegative O and carbonyl carbon C [reaction coordinate (RC)], varied within a range of 4.5–2.5 Å.

Every frame in the interpolation was followed by optimization, so that the distance between O and carbonyl carbon of the substrate remained unchanged: Namely, we assigned an explicit value to the RC O/C distance, while all other degrees of freedom were recalculated at each step. The translation step toward the nucleophilic center was set to 0.2 Å in each interpolation frame.

1. Otwinowski Z, Minor W (1996) Processing of X-ray diffraction data collected in oscillation mode. *Meth Enzymol* 276:307–326.

2. Mosyak L, Reshetnikova L, Goldgur Y, Delarue M, Safro MG (1995) Structure of phenylalanyl-tRNA synthetase from *Thermus thermophilus*. *Nat Struct Biol* 2(7):537–547.

3. Brünger AT, et al. (1998) Crystallography & NMR system: A new software suite for macromolecular structure determination. *Acta Crystallogr D Biol Crystallogr* 54(Pt 5): 905–921.
4. Jones TA, Zou JY, Cowan SW, Kjeldgaard M (1991) Improved methods for building protein models in electron density maps and the location of errors in these models. *Acta Crystallogr A* 47(Pt 2):110–119.
5. Stewart JJ (2007) Optimization of parameters for semiempirical methods V: Modification of NDDO approximations and application to 70 elements. *J Mol Model* 13(12): 1173–1213.
6. DeLano WL (2004) *PyMOL User's Guide* (DeLano Sci, Palo Alto, CA).
7. Pettersen EF, et al. (2004) UCSF Chimera—A visualization system for exploratory research and analysis. *J Comput Chem* 25(13):1605–1612.
8. Warshel A, Levitt M (1976) Folding and stability of helical proteins: Carp myogen. *J Mol Biol* 106(2):421–437.
9. Vreven T, et al. (2006) Combining quantum mechanics methods with molecular mechanics methods in ONIOM. *J Chem Theory Comput* 2(3):815–826.
10. Salomon-Ferrer R, Case DA, Walker RC (2013) An overview of the Amber biomolecular simulation package. *Wires Comput Mol Sci* 3(2):198–210.
11. Stewart JJP (2012) M*OPAC2012* (Comput Chem, Colorado Springs, CO). Available at OpenMOPAC.net.
12. Laio A, VandeVondele J, Rothlisberger U (2002) A Hamiltonian electrostatic coupling scheme for hybrid Car-Parrinello molecular dynamics simulations. *J Chem Phys* 116(16):6941–6947.

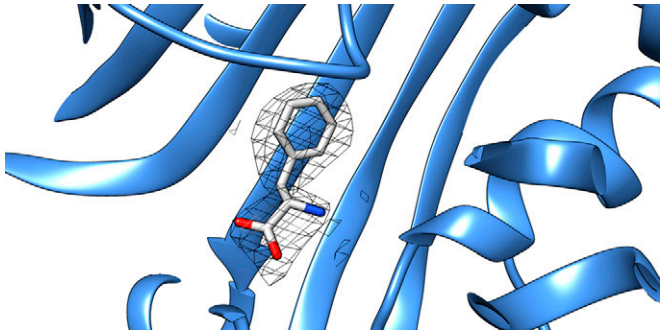

Fig. S1. The aminoacylation active site of the *Tt*PheRS with bound phenylalanine. The electron density map calculated as described in *Materials and Methods* is contoured at 3σ.

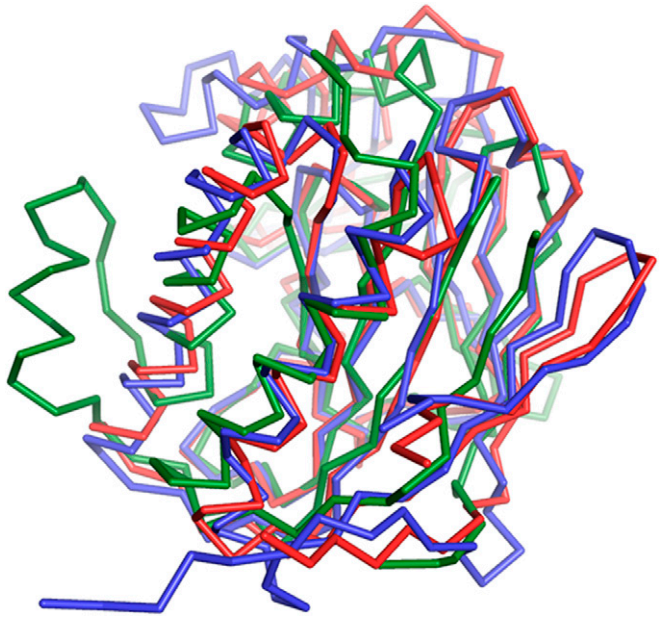

Fig. S2. Structural alignment of *Hs*PheRS (blue), *Ph*PheRS (red), and *Tt*PheRS (green) B3 editing subdomains.

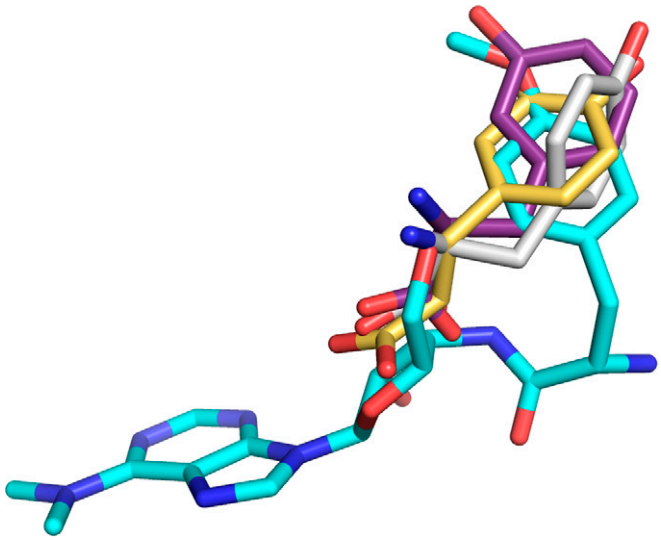

Fig. S3. Superposition of the puromycin, tyrosine, L-Dopa, and *meta*-tyrosine located in the editing site of *Tt*PheRS. Molecule of puromycin is colored cyan and blue, tyrosine is colored gray, L-Dopa is colored golden, and *meta*-tyrosine is colored purple. The aromatic rings of the ligands are rotated relative to each other and slightly shifted.

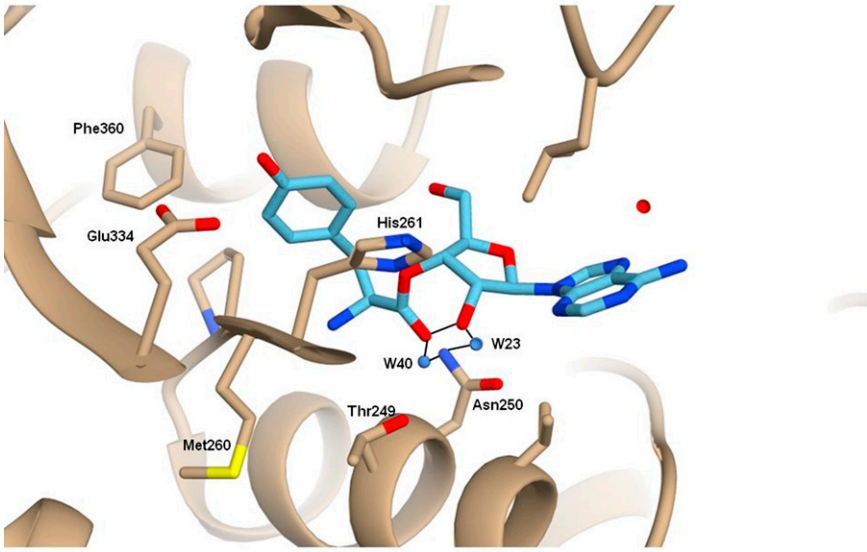

Fig. S4. Hydrogen bond network in the tyrosyl-3′-ribose complex. The ester oxygen (–O–) forms a weak hydrogen bond with protonated ND1 of His261. Conformation of the ester is also stabilized by the intramolecular hydrogen bond between the ribose O2′ and carbonyl oxygen. Two key hydrogen-bonded water molecules, W40 and W23, are involved in the interaction network around the ribose O2′.

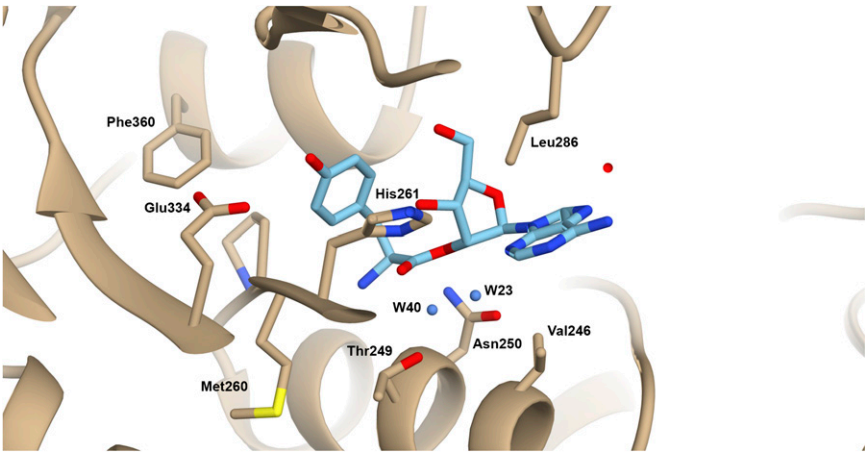

Fig. S5. Modeled structure of the tyrosyl-2′-ribose ester in the editing site of *Tt*PheRS. Visual comparison of tyrosyl-2′-ribose ester with that of tyrosyl-3′-ribose ester (Fig. S4) demonstrates remarkable plasticity of the editing site cavity. The positions of the amino acid residues embracing the isomeric ligands are kept virtually unchanged.

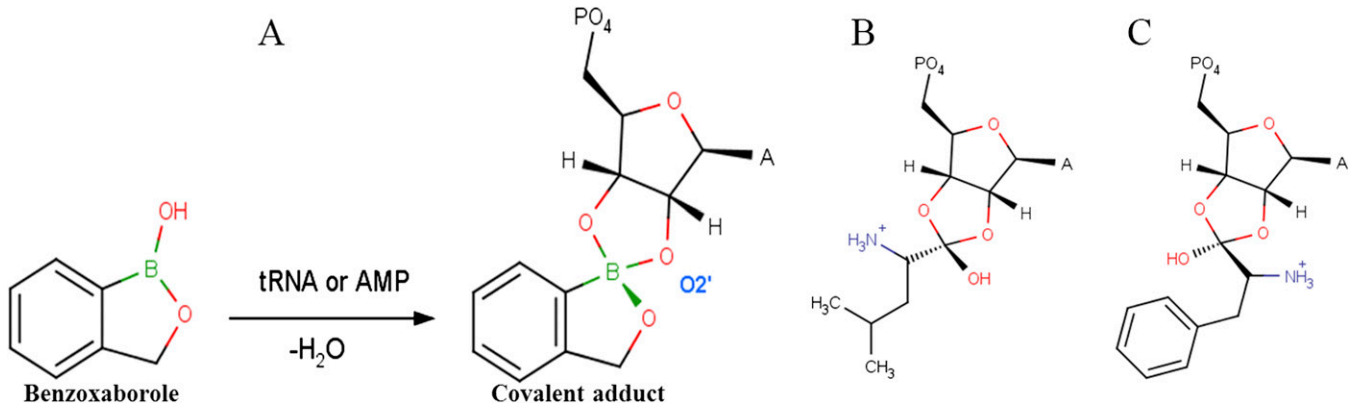

Fig. S6. Reaction between benzoxaborole and $tRNA^{Leu}$ or AMP. The 2′,3′-hydroxyl groups of the ribose covalently bind to the boron atom from the oxaborole ring, forming tetrahedral spiroborate structure. (*A*) An adduct to $tRNA^{Leu}$ (solid and hashed wedged bonds) is identical to that revealed in the editing site of LeuRS (PDB ID codes 2WFD, 4AS1, and 4ARI). (*B*) Leu-orthoester is the structural analog of the benzoxaborole adduct. (*C*) Phe-orthoester. Two configurations display different orientations of the labile hydroxyl at the chiral carbon center.

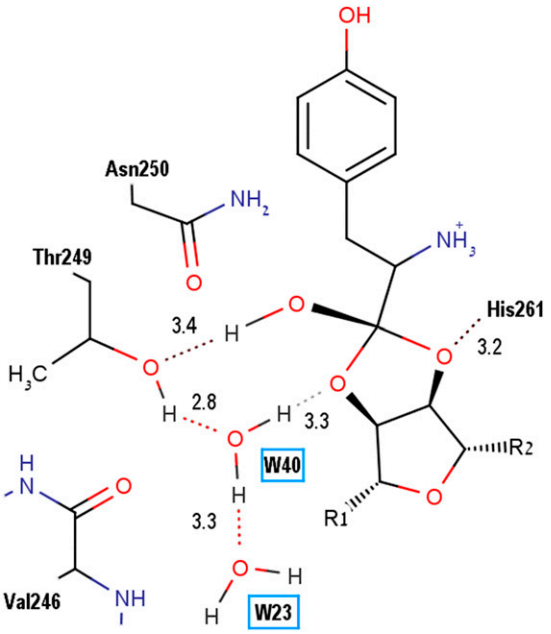

Scheme S1. The breaking of the HB between Thr249 and Val246.

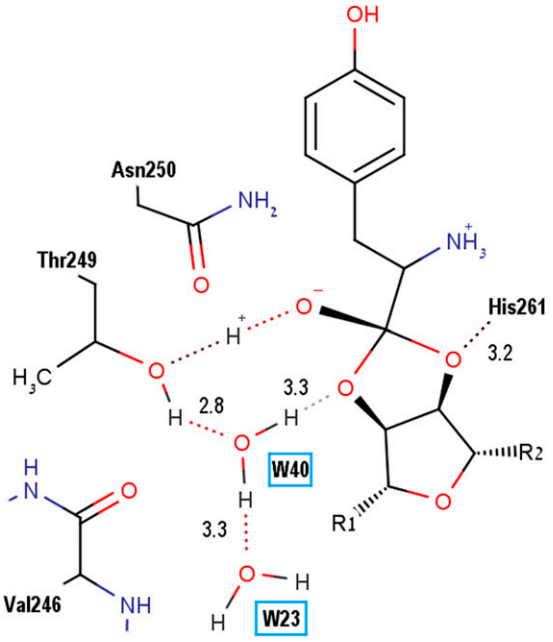

Scheme S2. Polarization of the labile hydroxyl ortho-OH, and proton exchange with Thr249.

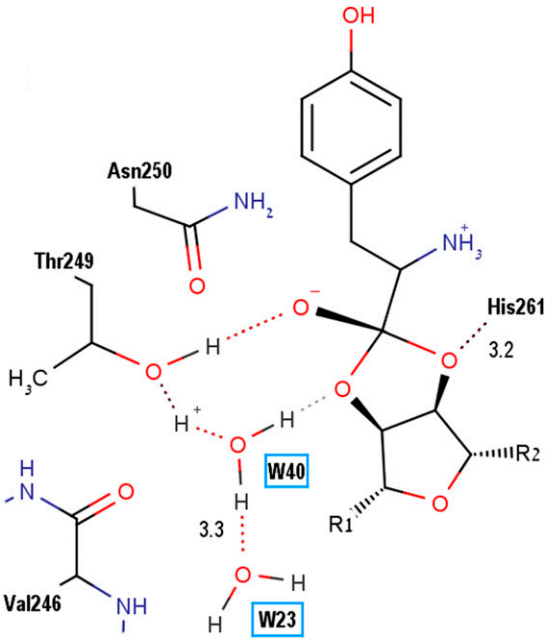

Scheme S3. The proton migration from Thr249 to W40.

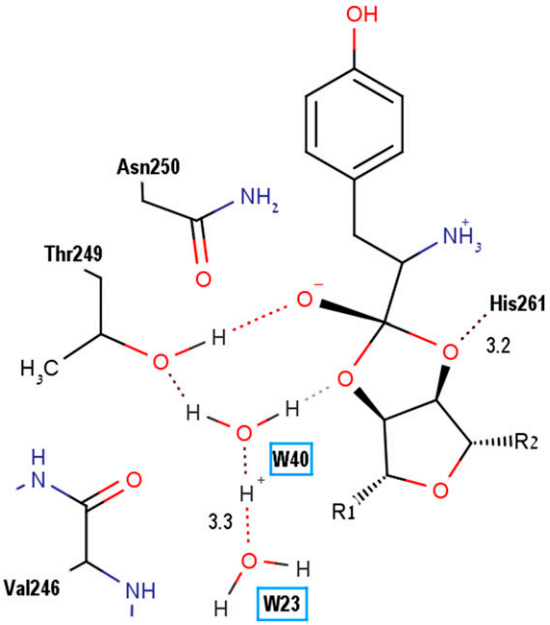

Scheme S4. Formation of the hydronium cation H5O2+.

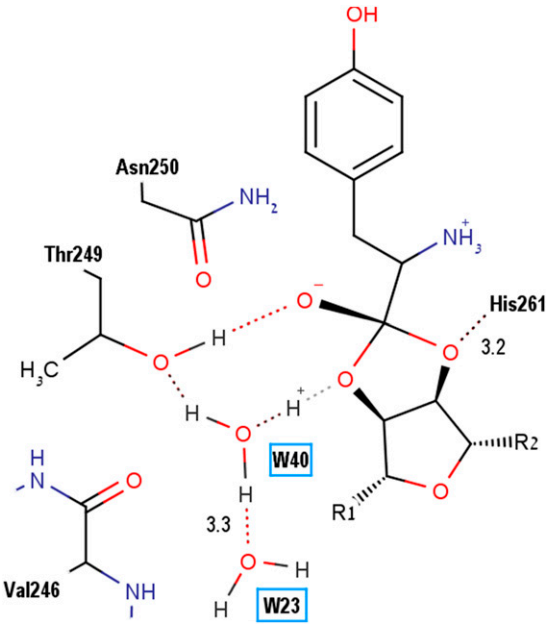

Scheme S5. The proton migration onto ribose O2′.

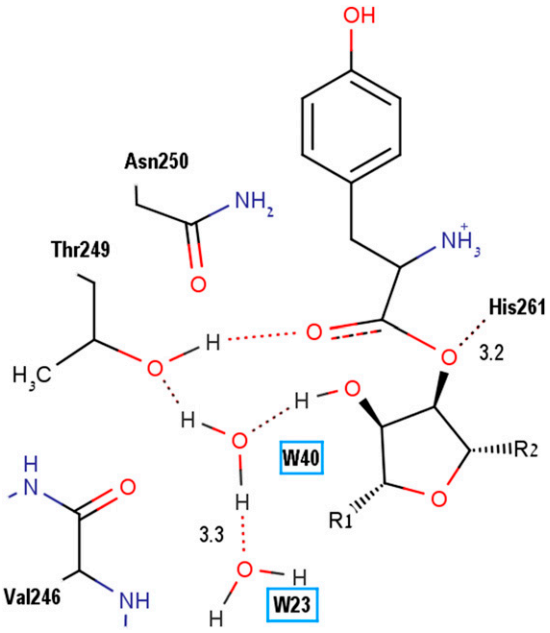

Scheme S6. The breaking of the cyclic bond in orthoester and formation of the 3′-ester.

Table S1. Data collection and refinement statistics

Data collection	
Space group	$P3_221$
a,b,c, Å	176, 176, 138
α, β, γ, degrees	90, 90, 120
Resolution, Å	2.6
R_{merge}	9.2
$\langle I \rangle / \langle \sigma(I) \rangle$	20.14
Completeness, %	100
Redundancy	3.2
Refinement	
Resolution, Å	2.6
No. of reflections	71500
R_{work}/R_{free}	29.6/26.4
No. of atoms	
Protein	8250
Ligands	45
Ions	1
Water	175
B factors	
Protein	62.0
Ligand	81.0
Water	48.0
rmsds	
Bond lengths, Å	0.0075
Bond angles, degrees	1.406

Data were collected from a single crystal.